Journal of Constructional Steel Research 166 (2020) 105910

Contents lists available at ScienceDirect

Journal of Constructional Steel Research

Stub column behaviour of heat-treated and galvanized RHS manufactured by different methods

Kamran Tayyebi, Min Sun *

Department of Civil Engineering, University of Victoria, Victoria, British Columbia V8P 5C2, Canada

ARTICLE INFO

Article history:
Received 28 July 2019
Received in revised form 3 December 2019
Accepted 13 December 2019
Available online xxxx

Keywords:
Rectangular hollow section
Hollow structural section
Galvanizing
Direct-formed
Continuous-formed
Heat treatment
High-strength steel
Stub column
Yield slenderness limit

ABSTRACT

A complementary study showed that hot-dip galvanizing can sometimes significantly change the residual stress properties of cold-formed rectangular hollow sections (RHS). Hot dipping the RHS specimens in a molten zinc bath maintained at 450 °C for 10 min provided a partial residual stress relief comparable to the onerous heat treatment specified in ASTM A1085 and CSA G40.20/G40.21. Hence, further research is needed to: (1) quantify the effects of galvanizing, and (2) determine the optimized heat treatment duration for a partial residual stress relief for improvement of column behaviour. In this study, the effects of galvanizing and heat treatments to different degrees on the stub column behaviour of cold-formed RHS has been investigated comprehensively for the first time, by means of 36 stub column tests. The RHS specimens were manufactured by two dominant cold-forming methods: (1) indirect-forming from circular to rectangular, and (2) direct-forming. The nominal yield stresses of the materials ranged from 350 to 690 MPa. The RHS stub column test matrix has 10 different width-to-thickness ratios and includes both nonslender and slender sections.

1. Introduction

The application of cold-formed and subsequently galvanized tubular steel structures in bridges, highways, transmission towers, and industrial plants has expanded over the years [1]. Since the service life of the zinc coating is in general longer than the design life of the structure it protects, galvanized steel structures are often maintenance-free [2]. To support the sustainable development agenda, recent investigations [3–5] have been performed on galvanized cold-formed hollow structural sections (HSS) to further facilitate their applications. It was found that, similar to heat treatment, the hot-dipping process (in a molten zinc bath maintained at 450 °C for approximately 10 min) can sometimes effectively lower the residual stress level and in return improve the column behaviour. However, these investigations did not cover a wide range of cross-sectional shapes, dimensions or material grades. The implications of using materials cold-formed by different approaches were not appreciated either. Hence, further research is needed to explore the potential benefits of hot-dip galvanizing on the structural behaviour of cold-formed HSS members.

In practice, the column behaviour of a cold-formed HSS member can be improved by specification of a heat treatment per ASTM A1085 Supplement S1 [6], or for a Class H finish per CSA G40.20/G40.21 [7]. Both standards describe identical heat treatment, at a temperature of 450 °C or higher, followed by cooling in air. The primary effect of the ASTM A1085 Supplement S1 and CSA G40.20/G40.21 Class H heat treatment is the provision of partial residual stress relief throughout the cross section. Such heat treatment justifies the use of a higher column curve in the Canadian steel design standard [8]. Due to the lack of definitive provisions in ASTM A1085 or CSA G40.20/G40.21, producers typically specify a holding time of 30 min once the furnace temperature is stable at 450 °C [1,5]. However, it was deduced by Sun and Ma [5] that a 10 min-holding time can release a similar amount of residual stress as a 30 min-holding time. In other words, a holding time of 30 min may be excessive for the purpose of improving column behaviour. Hence, further research is needed to determine the optimized temperature and duration, so that the heat treatment is fit-for-purpose and energy efficient.

This research focused on the effects of galvanizing and heat treatment on the stub column behaviour of cold-formed RHS. Previous research [9–13] showed that the mechanical behaviours of RHS manufactured by different cold-forming methods can sometimes be significantly different. Hence, in order to conduct a comprehensive investigation on the effects of the above post-cold-forming processes and develop general conclusions, the test matrix of this study included RHS cold-formed by different methods. In North America, square and rectangular hollow sections (collectively referred to as RHS herein) of commonly specified sizes are produced as cold-formed members by two methods: (i) “indirect-forming from circular to rectangular”, where the coil material is initially cold-formed into a circular section, and subsequently cold-shaped into a rectangular section; or (ii)

* Corresponding author.
E-mail address: msun@uvic.ca (M. Sun).

https://doi.org/10.1016/j.jcsr.2019.105910
0143-974X/

"direct-forming", where the coil material is directly cold-formed into a rectangular shape. Indirect-formed RHS is subjected to high degrees of cold-forming over the entire cross-section. For direct-formed RHS, the cold-forming is only concentrated at the corner regions. For this reason, the structural behaviours of indirect- and direct-formed RHS having similar appearances can sometimes be quite different. It should be noted that new generation of direct-formed high-strength RHS products with a nominal yield stress of 690 MPa are now readily available in the North American market. The new high-strength product contains inherently a low level of residual stress as a result of the unique manufacturing process [11–13]. Hence, its application can reduce the weight of the structure and save the cost of heat treatment. However, existing design specifications (e.g. [8,14]) do not distinguish the new products from the conventional hollow sections, hindering their widespread application in construction. Recent research efforts [15–21] have been made to study the structural performances of tubular members manufactured from high-strength steel coils with nominal yield stresses in the range of 460 to 1100 MPa. However, the RHS specimens included in these studies were indirect-formed. Hence, the results and conclusions cannot be directly applied to direct-formed RHS. Sun and Packer [11] investigated the mechanical behaviours of three direct-formed RHS specimens. However, no significant effort was made in [11] to study the effects of direct-forming on high-strength steel. In this research, a comprehensive study on the stub column behaviour of the new RHS product and the effects galvanizing and heat-treatment on it was performed for the first time.

The current experimental investigation examined the stub column behaviours of 14 high-strength direct-formed RHS specimens, 10 regular-strength direct-formed RHS specimens, and 12 regular-strength indirect-formed RHS specimens. Twenty one of the 36 RHS specimens were galvanized or heat-treated to different degrees. The stub column test results (e.g. proportional limits, local buckling stresses, yield stresses and ultimate stresses) of the RHS specimens were compared to study the effects of these post-cold-forming processes. The experimental compressive strengths were also compared to the design strengths calculated using equations set out in various design standards. In particular, since heat treatment and galvanizing can potentially reduce residual stress and in return delay local buckling, the test results from the slender cross sections before and after galvanizing were carefully compared. Since the compactness criteria in North American steel design standards [8,14] do not consider the effects of galvanizing or heat treatment, the results were also used to examine the compactness criteria in these design standards.

2. RHS specimens

In this study, a total of 13 cold-formed and untreated parent RHS (direct-formed or indirect-formed) were used to produce 36 RHS specimens subjected to different post-cold-forming treatments (untreated, galvanized, or heat-treated to a carefully controlled degree). Different from the previous research by Sun and Packer [11], which included only three external dimension-to-thickness ratios, and did not consider the effects of galvanizing and heat treatment at different temperatures, the current study included 36 RHS specimens having10 different external dimension-to-thickness ratios, among which 21 specimens were galvanized or heat-treated to different degrees.

Eight of the 13 parent RHS were regular-strength, and were manufactured to CSA G40.20/40.21 Gr. 350 W Class C [7]. The other five parent RHS were high-strength and direct-formed. The 36 RHS specimens were then used to produce a total of 36 stub columns and 112 tensile coupons. The stub column specimens are listed in Table 1.

Table 1
Dimensions of RHS Stub column specimens.

Stub column ID	B (mm)	H (mm)	t (mm)	r (mm)	L (mm)	A (mm^2)	B_n/t_n	H_n/t_n
DH-76 × 76 × 4.8-U	76.3	76.6	4.81	8.5	352	1303	16	16
DH-76 × 76 × 4.8-G								
DH-76 × 102 × 3.2-U	76.9	102.6	3.02	2.6	403	961	24	32
DH-76 × 102 × 3.2-G								
DH-76 × 102 × 3.2-U[a]								
DH-76 × 102 × 3.2-G[a]								
DH-76 × 102 × 4.1-U	76.3	101.8	4.06	4.8	402	1252	19	25
DH-76 × 102 × 4.1-G								
DH-76 × 102 × 4.8-U	76.6	102.0	4.82	8.9	402	1471	16	21
DH-76 × 102 × 4.8-G								
DH-76 × 152 × 4.1-U	77.2	153.1	4.04	5.1	503	1639	19	37
DH-76 × 152 × 4.1-G								
DH-76 × 152 × 4.1-U[a]								
DH-76 × 152 × 4.1-G[a]								
D-76 × 102 × 3.2-U	76.5	101.9	3.03	2.4	402	994	24	32
D-76 × 102 × 3.2-G								
D-76 × 102 × 4.8-U	76.4	101.9	4.36	3.4	404	1445	16	21
D-76 × 102 × 4.8-G								
D-102 × 102 × 3.2-U	101.1	101.9	3.03	3.4	402	1142	32	32
D-102 × 102 × 3.2-G								
D-102 × 102 × 4.8-U	101.6	102.1	4.40	5.6	403	1671	21	21
D-102 × 102 × 4.8-G								
D-127 × 127 × 4.8-U	127.0	127.6	4.40	6.6	403	2123	26	26
D-127 × 127 × 4.8-G								
I-102 × 102 × 6.4-U	102.1	102.2	6.41	8.0	350	2253	16	16
I-102 × 102 × 6.4–450								
I-102 × 102 × 6.4–595								
I-102 × 102 × 6.4-G								
I-102 × 102 × 7.9-U	101.9	102.1	7.83	11.7	350	2735	13	13
I-102 × 102 × 7.9–450								
I-102 × 102 × 7.9–595								
I-102 × 102 × 7.9-G								
I-102 × 102 × 13-U	101.6	101.7	12.90	11.8	350	4180	8	8
I-102 × 102 × 13–450								
I-102 × 102 × 13–595								
I-102 × 102 × 13-G								

[a] Indicates repeated test.

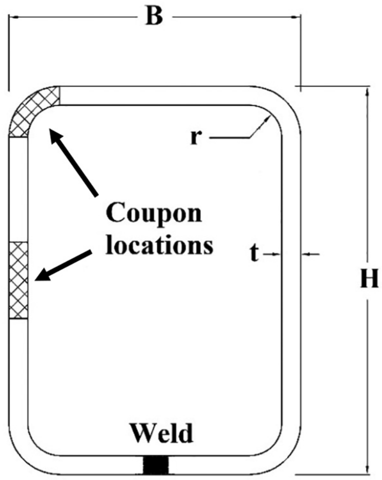

Fig. 1. Locations of tensile coupons.

As shown, the nominal external dimensions of the specimens varied from 76 to 152 mm, and the nominal wall thicknesses varied from 3.2 to 13 mm. Hence, the selected RHS covered a wide range of external dimension-to-thickness ratios, corresponding to a wide range of overall (cross-sectional) degrees of cold-working. Each stub column specimen in Table 1 is assigned an ID consisted of three components. The first component distinguishes the material by its cold-forming method and strength grade, where "DH" represents direct-formed high-strength RHS with a nominal yield stress of 690 MPa, while "D" and "I" represent direct-formed and indirect-formed RHS with a nominal yield stress of 350 MPa, respectively. The second component shows the nominal dimensions of the parent tube (width×height×wall thickness in mm). The third component indicates the type of post-cold-forming treatment applied to the specimens, where U = as-received untreated cold-formed RHS; G = hot-dip galvanizing at 450 °C for a duration of 10 min; 450 = heat treatment at 450 °C according to CAN/CSA G40.20/G40.21 for a Class H finish [7] or ASTM A1085 by specifying Supplement S1 [6]; and 595 = heat treatment at an annealing temperature of 595 °C per ASTM A143 [22]. It should be noted that the heat treatment at both 450 and 595 °C temperatures had a holding time of 30 min in furnace based on the current industrial practice. Prior to the experimental program, the cross-sectional dimensions of all sections were carefully measured using the approach adopted by [5,11] and are summarized in Table 1. The nominal dimensions, as indicated by a subscript "n", are used to calculate the external dimension-to-thickness ratios. As can be seen from Table 1, the effects of galvanizing and heat treatment to different degrees can be directly studied. Moreover, with the carefully selected specimens, the effect of different coil material grades can be directly studied [e.g. DH-76 × 102 × 3.2 (U and G) vs. D-76 × 102 × 3.2 (U and G); and DH-76 × 102 × 4.8 (U and G) vs. D-76 × 102 × 4.8 (U and G)]. Also, the effect of different cold-forming processes can be directly studied using specimens with similar cross-sectional dimensions [e.g. D-102 × 102 × 4.8 (U and G) vs. I-102 × 102 × 6.4 (U and G)].

3. Material properties

3.1. Tensile coupon tests

The material properties of the 36 RHS specimens were obtained tensile coupon tests. Flat coupons and corner coupons were machined from the cross sections. The locations of the tensile coupons are shown in Fig. 1. The dimensions of the flat coupons and the testing procedures adopted were in compliance with ASTM E8 [23]. An MTS 810 testing machine with a capacity of 250 KN was used. For testing of the corner coupons, based on the approach suggested by [24–26], a pair of pin-loaded connectors were employed. Holes were drilled in the grips of the curved coupons, and tensile loading was applied from the MTS machine to the coupon via the connector (See Fig. 2). The loading was applied at a displacement rate of 0.1 mm/min. An extensometer was used to record the elongation of the testing region of the coupons. Strain gauges were also employed to cross reference the extensometer readings. The readings agree well. Hence, credence was given to the accuracy of the tensile coupon test results. An overview of the test setup is shown in Fig. 2.

3.2. Discussion of tensile test results

Typical tensile stress-strain curves of the direct- and indirect-formed RHS materials are shown in Figs. 3 and 4, respectively. As shown, the corner coupons of the cold-formed and untreated RHS, whether direct-formed or indirect-formed, had rounded stress-strain responses with no sharply defined yield point. Similar responses were observed for the flat coupons of the indirect-cold-formed and untreated RHS, since the flat face materials were also heavily cold-worked during the two-step rolling process. On the other hand, the curves for the flat faces of the direct-cold-formed RHS are less rounded and in general have much higher proportional limits, indicating a much lower level of cold-working at these locations. Since tube manufacturers in general emphasize on achieving a reliably large flat width dimension, it can be

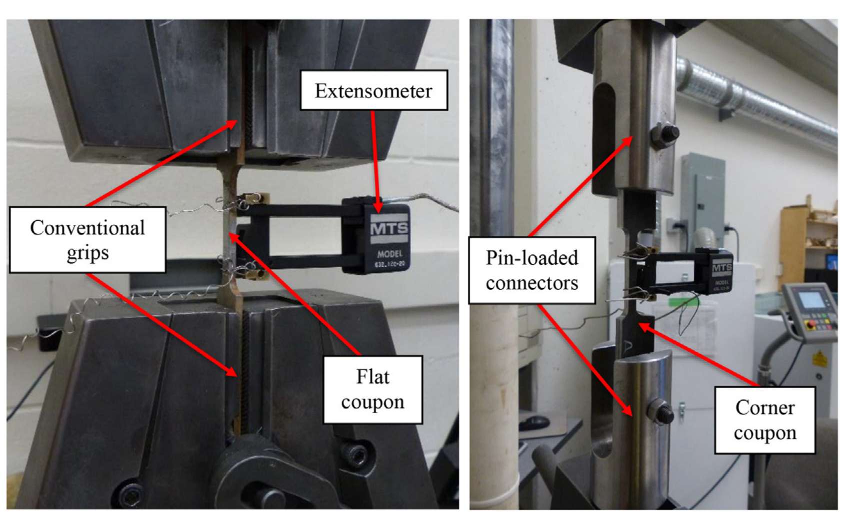

Fig. 2. Test setup for the flat and corner coupons.

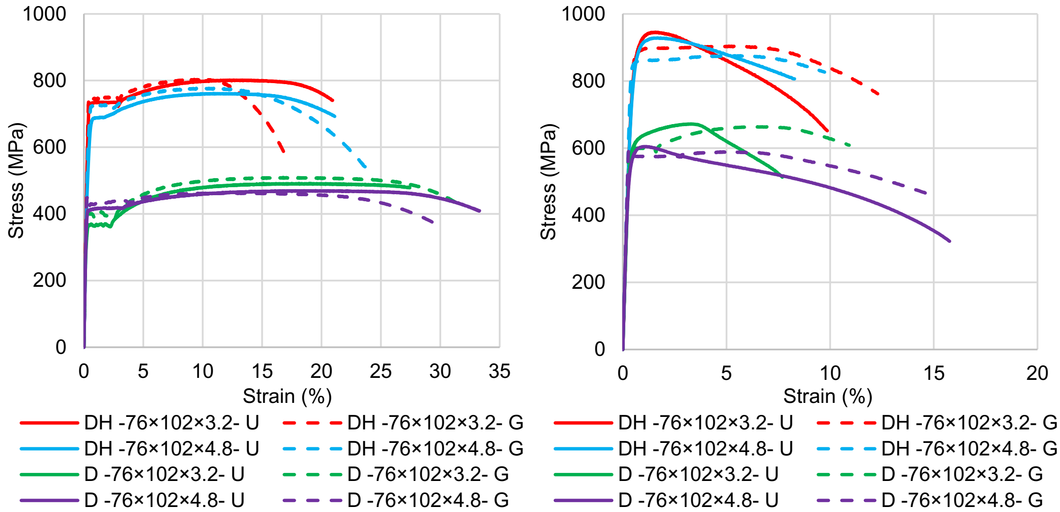

(a) Flat coupon (b) Corner coupon

Fig. 3. Typical tensile stress-strain curves of direct-formed regular- and high-strength RHS.

deducted that a direct-formed RHS contains a much lower overall (cross-sectional) level of residual stress than its indirect-formed counterpart.

One important finding of the tensile coupon tests is that the hot-dip galvanizing process is very effective in reducing the residual stress levels. As shown in Figs. 3 and 4, the curves for the coupons machined from the galvanized RHS specimens in general showed clear yield plateaus. Another important finding, as clearly shown in Fig. 4, is that the effect of hot-dipping, with a ten-minute duration, is very similar to the onerous heat treatment specified in ASTM A1085 S1 [6] and CSA G40.20/40.21 [7], which includes: (i) increasing the furnace containing the cold-formed hollow section materials to 450 °C or higher; (ii) holding the furnace temperature for 30 mins; and (iii) cooling the materials to ambient temperature. The same phenomenon was observed in the stub column tests, which will be discussed in Section 5. Hence, comprehensive research is needed in this regard to optimize the current practice for post-cold-forming heat treatment (for improvement of column behaviour) so that it is fit-for-purpose and energy efficient. On the other hand, a clear trade-off between yield strength and residual stress level can be observed by comparing the materials heat treated to 595 °C to their untreated counterparts.

All of the above conclusions are further substantiated by analysing the average values of the key test results of all tensile coupons in Table 2, including the Young's modulus (E), yield stress (σ_y), ultimate stress (σ_u), and rupture strain (ε_r). Subscripts "f" and "c" were added to the labels to differentiate the flat and corner coupons. The yield stress was determined using the 0.2% strain offset method. Similar to the commonly applied post-cold-forming heat treatment at 450 °C for partial residual stress relieving (e.g. for a Class H finish per [7]), the application of hot-dip galvanizing in general has minor effects on (slightly increased) the yield and ultimate strengths of the cold-formed and untreated materials, regardless of the strength grades. On the other hand, for the 595 °C heat treatment, the trade-off between strength and ductility should be considered by the engineers and fabricators when specifying this post-cold-forming heat treatment.

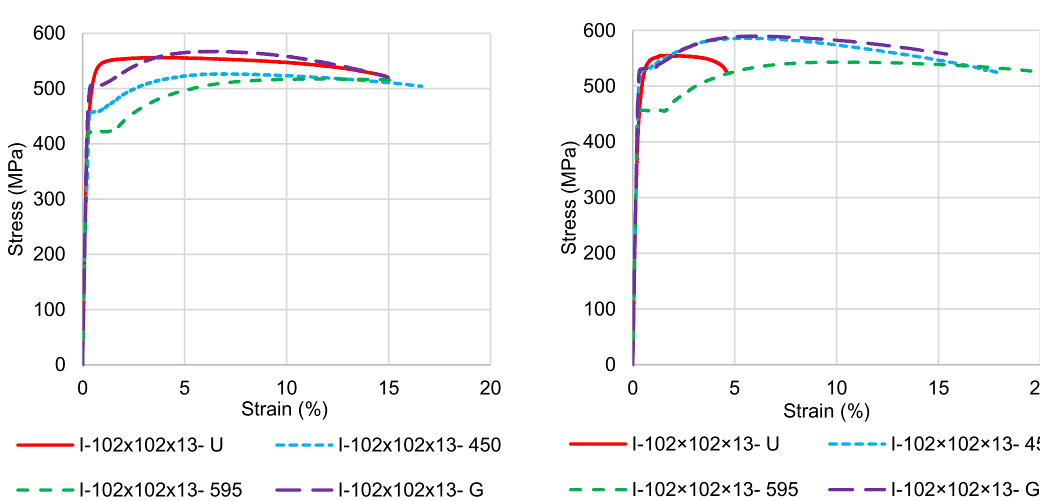

(a) Flat coupon (b) Corner coupon

Fig. 4. Typical stress-strain curves of indirect-formed regular-strength RHS.

Table 2
Average tensile coupon test results.

Specimen ID	Corner coupons					Flat coupons					$\frac{\sigma_{y,c}}{\sigma_{y,f}}$	$\frac{\varepsilon_{r,c}}{\varepsilon_{r,f}}$
	$\sigma_{p,c}$ (MPa)	E_c (GPa)	$\sigma_{y,c}$ (MPa)	$\sigma_{u,c}$ (MPa)	$\varepsilon_{r,c}$ (%)	$\sigma_{p,f}$ (MPa)	E_f (GPa)	$\sigma_{y,f}$ (MPa)	$\sigma_{u,f}$ (MPa)	$\varepsilon_{r,f}$ (%)		
DH-76 × 76 × 4.8-U	360	190	789	863	19	330	199	638	767	27	1.24	0.70
DH-76 × 76 × 4.8-G	420	229	878	893	22	450	203	743	786	28	1.18	0.79
DH-76 × 102 × 3.2-U	520	206	862	945	12	340	217	730	802	27	1.18	0.44
DH-76 × 102 × 3.2-G	680	207	876	904	14	580	217	742	803	20	1.18	0.70
DH-76 × 102 × 4.1-U	430	211	879	960	12	350	202	692	776	26	1.27	0.46
DH-76 × 102 × 4.1-G	760	227	901	909	17	420	202	711	792	26	1.27	0.65
DH-76 × 102 × 4.8-U	560	206	849	928	16	350	194	651	761	29	1.30	0.55
DH-76 × 102 × 4.8-G	670	225	816	876	20	520	191	720	777	26	1.13	0.77
DH-76 × 152 × 4.1-U	420	204	930	1054	14	300	198	713	815	30	1.30	0.47
DH-76 × 152 × 4.1-G	730	222	918	949	16	460	208	744	819	28	1.23	0.57
D-76 × 102 × 3.2-U	360	200	601	672	14	175	203	367	492	34	1.64	0.41
D-76 × 102 × 3.2-G	500	208	599	664	16	280	211	400	509	32	1.50	0.50
D-76 × 102 × 4.8-U	320	217	568	605	18	225	200	409	470	39	1.39	0.46
D-76 × 102 × 4.8-G	510	225	574	595	20	280	204	424	463	36	1.35	0.56
D-102 × 102 × 3.2-U	230	220	567	623	15	220	203	344	469	32	1.65	0.47
D-102 × 102 × 3.2-G	320	223	536	638	15	310	198	380	497	32	1.41	0.47
D-102 × 102 × 4.8-U	300	206	574	618	18	260	205	399	487	38	1.44	0.47
D-102 × 102 × 4.8-G	550	218	596	620	20	320	219	470	515	30	1.27	0.67
D-127 × 127 × 4.8-U	220	213	553	588	16	190	202	395	457	40	1.40	0.40
D-127 × 127 × 4.8-G	460	223	574	603	22	310	200	427	468	37	1.34	0.59
I-102 × 102 × 6.4-U	180	198	496	544	14	170	199	415	482	30	1.2	0.47
I-102 × 102 × 6.4–450	510	199	550	610	21	350	201	427	505	31	1.29	0.68
I-102 × 102 × 6.4–595	360	198	434	502	26	350	200	384	486	33	1.13	0.79
I-102 × 102 × 6.4-G	390	200	508	554	16	360	203	445	509	27	1.14	0.59
I-102 × 102 × 7.9-U	260	201	539	577	14	210	198	458	509	25	1.18	0.56
I-102 × 102 × 7.9–450	485	205	566	629	21	420	208	468	539	26	1.21	0.81
I-102 × 102 × 7.9–595	460	202	485	559	25	390	206	409	505	31	1.19	0.81
I-102 × 102 × 7.9-G	440	201	539	590	17	400	194	478	530	22	1.13	0.77
I-102 × 102 × 13-U	240	198	506	563	14	150	201	483	549	22	1.05	0.64
I-102 × 102 × 13–450	390	201	528	592	19	250	201	480	566	25	1.10	0.76
I-102 × 102 × 13–595	425	204	459	546	26	380	196	433	527	30	1.06	0.87
I-102 × 102 × 13-G	405	206	538	596	17	360	207	493	555	25	1.09	0.81

As discussed previously, the cross-sectional dimensions of the RHS were carefully selected so that direct comparisons among the specimens could be made. All indirect-formed RHS have the same external dimensions but different wall thicknesses. As shown in Table 2, for the three indirect-cold-formed and untreated RHS specimens, as the wall thickness increases, the $\sigma_{y,c}/\sigma_{y,f}$ - ratio decreases and the $\varepsilon_{y,c}/\varepsilon_{y,f}$ - ratio increases. This shows that, as the external dimension-to-thickness ratios increases, the amount of cold-working over different regions of an indirect-cold-formed cross section becomes more uniform. On the other hand, for the direct-formed RHS specimens, high $\sigma_{y,c}/\sigma_{y,f}$ - ratios and low $\varepsilon_{y,c}/\varepsilon_{y,f}$ - ratios were observed for all cross sections with different external dimension-to-thickness ratios, which imply that the cold-working is only concentrated at the corner regions.

4. Geometric imperfections

As a result of the manufacturing processes such as roll forming, most structural steel members have initial geometric imperfections, including local and global out-of-straightness in the perpendicular directions to the member surfaces [8,14]. The buckling response and load carrying capacity of a steel member under compression is influenced by its geometric imperfections. In this study, the magnitude and distribution of the initial imperfections of all four faces of sections cold-formed by different methods were determined using the seven representative RHS stub column specimens listed in Table 3. The measurements were performed on all three sizes of the indirect-formed RHS, and four direct-formed RHS to cover a wide range of external dimension-to-thickness ratios. As shown in Fig. 5, the setup consisted of a milling machine worktable on which the specimens were firmly clamped. The worktable provided a flat reference surface for the measurements. A digital Linearly Varying Displacement Transducer (LVDT), with an accuracy of 0.002 mm, was mounted to the head of the milling machine to measure the imperfections, as recommended by [15,16,27–29]. To exclude the possible local distortions due to cold sawing at the ends of the specimens, the starting and finishing points for the measurements were selected to be 30 mm away from the ends [17]. The worktable and the RHS specimen moved together in the longitudinal direction, which allowed the stationary LVDT to capture the imperfections along the 12 lines of interest shown in Fig. 6. On each face of an RHS, two of the lines were located near the corners, and a third one

Table 3
Results of geometric imperfection measurements.

Specimen ID	δ_{max}	Section slenderness ratio $\alpha = (H - 2R)/t$	$\lvert\delta_{max}/t\rvert$ (%)	$\lvert\delta_{max}/\alpha\rvert$ (mm)	$\lvert(\delta_{max}/\alpha)\rvert_{avg}$ (mm)
DH -76 × 76 × 4.8- U	0.356	10.4	7.4	0.034	0.023
DH -76 × 152 × 4.1- U	0.376	33.4	9.3	0.011	
D-76 × 102 × 4.8- U	−0.172	19.8	3.9	0.009	0.014
D-102 × 102 × 3.2- U	0.602	29.4	20.0	0.020	
I-102 × 102 × 6.4- U	0.314	11.4	4.9	0.027	0.090
I-102 × 102 × 7.9- U	0.294	8.1	3.7	0.036	
I-102 × 102 × 13- U	0.836	4.0	6.5	0.206	

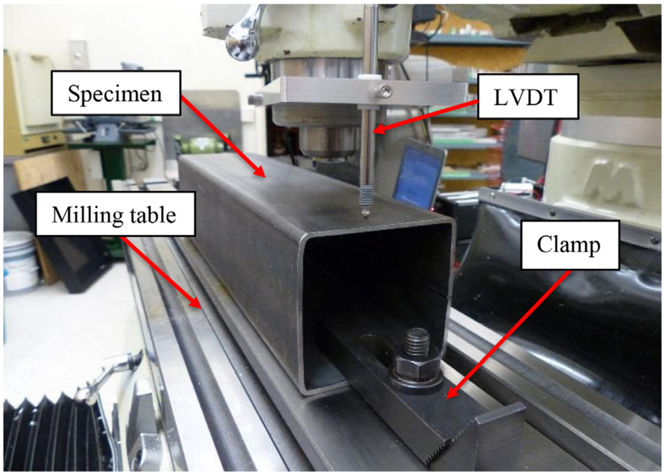

Fig. 5. Test setup for geometric imperfection measurements.

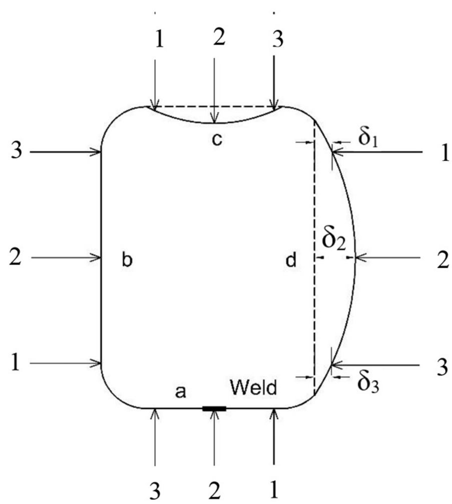

Fig. 6. Locations of geometric imperfection measurements.

at the centreline of the flat face. The difference between the centreline reading (δ_1) and the average of the two near- the-corner readings (δ_1 and δ_3) was calculated and taken as the imperfection at the measured location. This procedure, which recurred at every 5 mm along the entire length of each specimen, was repeated on all four faces. The maximum imperfection (δ_{max}) of all measured values of the seven RHS specimens are listed in Table 3.

Table 3 summarizes the key values of the measured magnitudes of the initial imperfections of the seven representative RHS specimens. The geometric imperfection profiles along the lengths of three representative RHS specimens are shown in Figs. 7–9, including one indirect-formed, one direct-formed and one direct-formed high-strength RHS of similar cross-sectional dimensions. Faces a to d in these graphs are consistent with those shown in in Figs. 7–9, a positive value represents a convex deformation, whereas a negative value represents a concave deformation. It can be seen from the figures that the initial geometric imperfections of the three representative RHS specimens are in general in the same order, regardless of the cold-forming approach used. The maximum local imperfection (δ_{max}) of the seven RHS specimens are listed in Table 3. The δ_{max}/t-ratios were also tabulated. Previous research [17,29] suggested that δ_{max} is also proportional to the cross section slenderness. Hence the δ_{max} values were also normalized in Table 3 by $\alpha = (H - 2R)/t$, where H and R are the depth and the outside corner radius of the corresponding RHS. These correlations can easily be used in finite element modelling of the stub columns.

5. Stub column tests

The 36 stub column specimens in Table 1 were prepared and tested following the widely accepted recommendations documented in the Structural Stability Research Council (SSRC) guide [30]. The lengths of the stub columns were selected to be at least three times the larger external dimension, but no >20 times the smaller radius of gyration. This ensures a realistic inclusion of the initial geometric imperfections and residual stresses, while minimizing the likelihood of global buckling. After cutting a stub column into the desired length, both ends were machined flat and normal to the tube's longitudinal axis. Compression tests were conducted using an MTS universal testing machine with a force capacity of 2000 kN. A spherical bearing was installed under the bottom bearing platen to ensure alignment, and to remove any gap between the bearing platens and the specimen ends. Fig. 10. shows the stub column test setup. Quasi-static displacement-controlled loading was applied at a rate of 0.5 mm/min. Four LVDTs were arranged next to each flat face to determine the average end shortening. Strain gauges were installed on all faces of all stub columns. An HBM data acquisition system and the CATMAN software package were used to record and log the strain gauge readings at one-second intervals. The strain gauge readings were monitored in real time to ensure alignment of

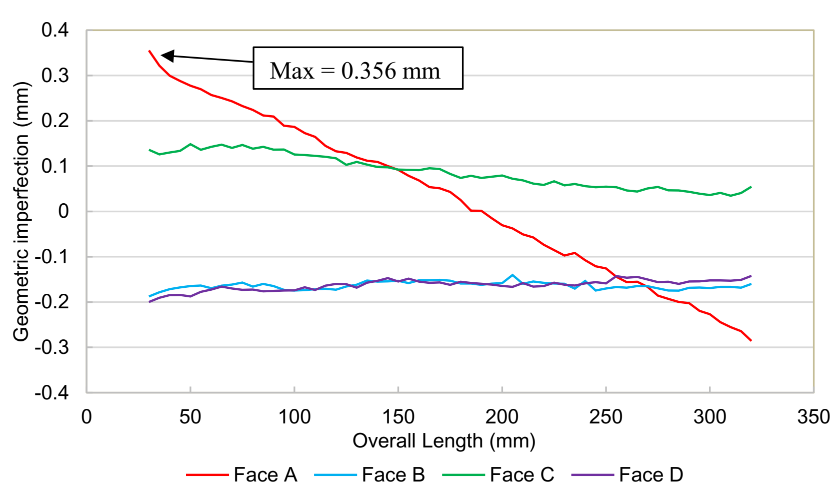

Fig. 7. Local geometric imperfection profiles of DH-76 × 76 × 4.8-U.

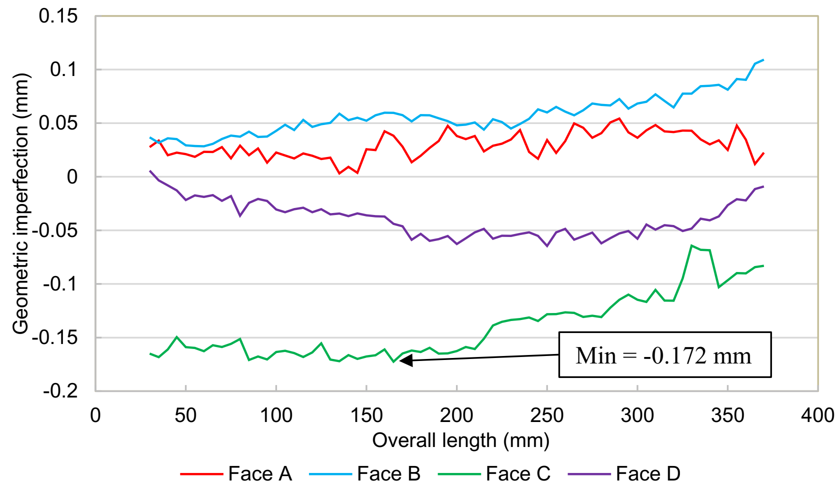

Fig. 8. Local geometric imperfection profiles of D-76 × 102 × 4.8-U.

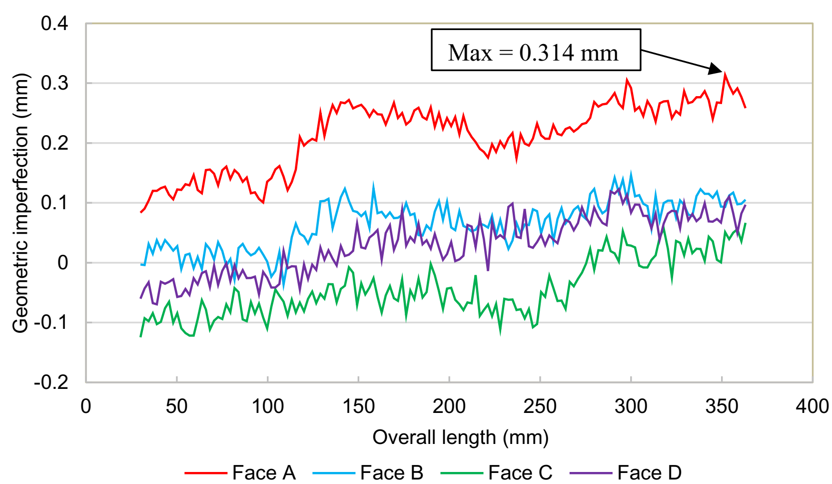

Fig. 9. Local geometric imperfection profiles of I-102 × 102 × 6.4-U.

the stub column specimens, and also to determine the onset of local buckling.

Representative stub column test results are shown in Fig. 11. The compressive stress was determined by dividing the axial load by the cross-sectional area. The cross-sectional area was measured through dividing the weight of each specimen by its length and the density of steel (taken as 7850 kg/m^3 [8]). The axial strain was calculated by dividing the average end shortening based on the LVDT readings by the initial length of the specimen. According to the stress-strain curves, nonslender sections in general reached cross-sectional yielding (CY in Table 4) and exhibited pronounced strain hardening responses. On the other hand, responses of slender sections showed early initiation of local buckling (LB in Table 4), followed by rapid loss of load carrying capacity. Similar to the findings from the tensile coupon tests, the stub column results herein further substantiated that both hot-dip galvanizing and heat treatment can effectively reduce residual stresses, and increase the uniformity of material properties around the section [3–5,11]. A shown in Fig. 11(c) and (d), the compressive stress-strain curves of the hot-dip galvanized specimens and the specimens heat-treated at 450 °C are comparable. The key results of the stub column tests are summarized in Table 4. The cross-sectional compressive yield stress was measured using the 0.2% strain offset method. The Young's modulus was determined based on the average strain gauge data in the linear elastic range. In Table 4, the cross-sectional compressive yield and ultimate stresses were compared to their corresponding tensile yield and ultimate stresses of the flat tensile coupons ($\sigma_{y,f}$ and $\sigma_{u,f}$). As shown by the

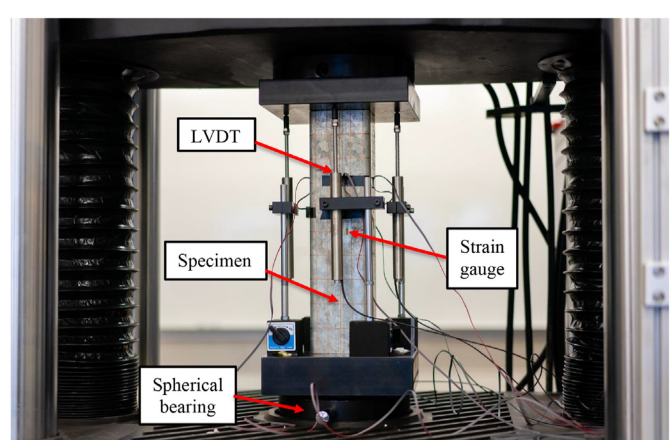

Fig. 10. Stub column test setup.

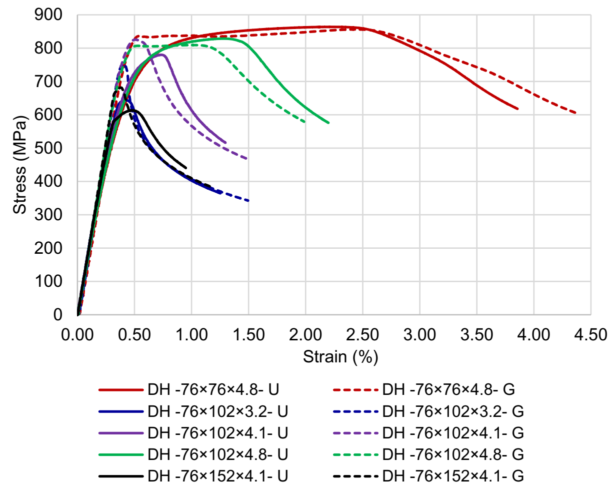

(a) Untreated and galvanized direct-formed high-strength RHS specimens

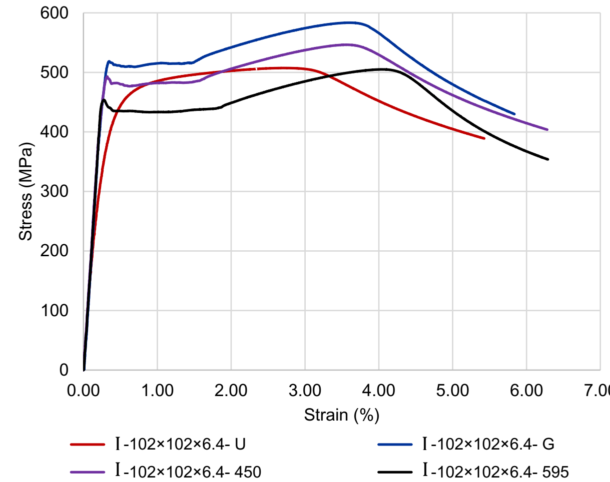

(c) Untreated, galvanized, and heat-treated indirect-formed regular-strength RHS 102×102×6.4

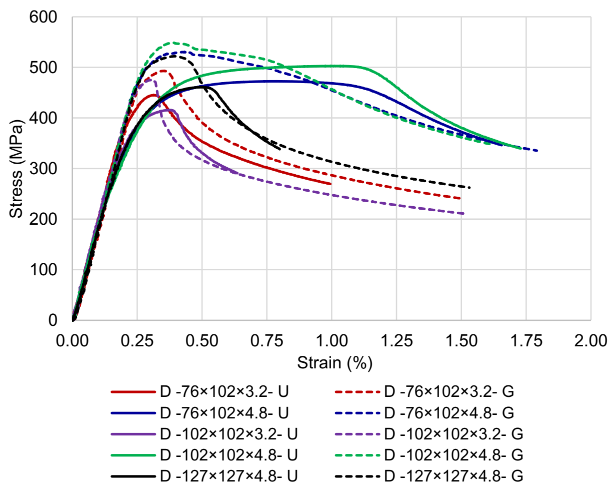

(b) Untreated and galvanized direct-formed regular-strength RHS specimens

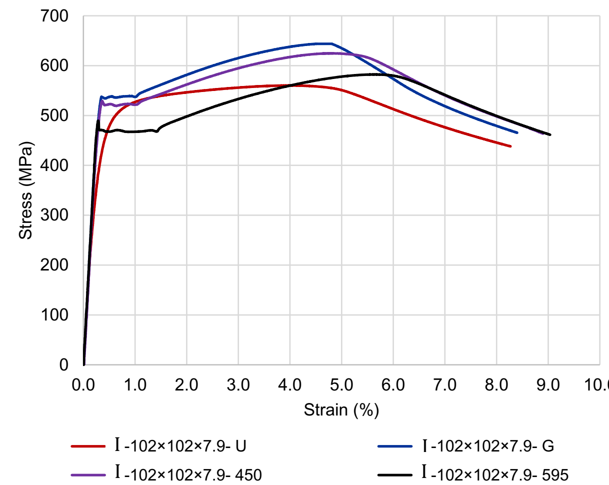

(d) Untreated, galvanized, and heat-treated indirect-formed regular-strength RHS 102×102×7.9

Fig. 11. Representative stub column test results.

comparisons, due to the strength enhancement at the corner regions, the cross-sectional compressive yield and ultimate stresses are in general higher for the nonslender sections. Four of the indirect-formed specimens with a 13-mm nominal wall thickness had squash loads higher than the capacity of the MTS machine (2000 kN). In these cases, attempts were made to determine the proportional limits of the four specimens.

5.1. Stub column strengths

By comparing the stub column test results of the 15 untreated RHS specimens (including RHS cold-formed by different methods and the repeated tests) with their 15 galvanized counterparts in Table 4, it was found that the hot-dipping process (with a duration of 10 min) increased on average the cross-sectional yield stress by 13%. This is consistent with the experimental observations by [4,5]. As shown by the experimental evidence discussed in Section 3.2, the galvanizing process had minor effects on the material yield stress based on the tensile coupon test results. Hence, the increase in the stub column load carrying capacity (i.e. the increase in the cross-sectional yield stress) is mainly due to the effective reduction of residual stress levels. Due to the same reason, the galvanizing process increased on average the cross-sectional ultimate stress by 11% based on the results in Table 4. Similar to hot-dip galvanizing, heat treatment at 450 °C (with a holding time of 30 min based on the current practice) on average increased the cross-sectional yield and ultimate stresses of the untreated Class C indirect-formed RHS by 12% and 10%, respectively. Hence, the holding time used in the current practice for an ASTM A1085 S1 finish [6], or a CSA G40.20/40.21 Class H finish [7] may be excessively long. In other words, the improvement on column behaviour may be very marginal after a ten-minute holding time.

On the other hand, heat treatment at 595 °C was shown to have a negligible influence on the load carrying capacities of the stub column specimens. This is because, although the 595 °C heat treatment is very effective in lowering the residual stress levels, such improvement is offset by the reduction in material yield and ultimate stresses. This is consistent with the findings from the tensile coupon tests. Hence, the 595 °C heat treatment per ASTM A143 [22], which consumes more energy than the 450 °C heat treatment per [6,7], should not be specified for improvement of column behaviour.

Table 4
Key stub column test results.

Specimen ID	E (GPa)	σ_y (MPa)	σ_u (MPa)	σ_p (MPa)	σ_{lb} (MPa)	Failure mode	$\sigma_y/\sigma_{y,f}$	$\sigma_u/\sigma_{u,f}$	$\sigma_{lb}/\sigma_{y,f}$	$\sigma_p/\sigma_{y,f}$
DH -76 × 76 × 4.8- U	202	754	864	320	N/A	CY	1.18	1.13	N/A	0.50
DH -76 × 76 × 4.8- G	217	833	856	650	N/A	CY	1.12	1.09	N/A	0.87
DH -76 × 102 × 3.2- U	209	643	643	310	625	LB	0.88	0.80	0.86	0.42
DH -76 × 102 × 3.2- G	228	755	755	620	N/A	CY	1.02	0.94	N/A	0.84
DH -76 × 102 × 3.2- U[a]	213	661	661	310	640	LB	0.91	0.82	0.88	0.42
DH -76 × 102 × 3.2- G[a]	225	765	765	670	N/A	CY	1.03	0.95	N/A	0.90
DH -76 × 102 × 4.1- U	205	757	780	350	N/A	CY	1.09	1.01	N/A	0.51
DH -76 × 102 × 4.1- G	223	829	829	660	N/A	CY	1.17	1.05	N/A	0.93
DH -76 × 102 × 4.8- U	209	756	828	325	N/A	CY	1.16	1.09	N/A	0.50
DH -76 × 102 × 4.8- G	220	806	811	600	N/A	CY	1.12	1.04	N/A	0.83
DH -76 × 152 × 4.1- U	209	613	613	325	570	LB	0.86	0.75	0.80	0.46
DH -76 × 152 × 4.1- G	221	687	687	650	660	LB	0.92	0.84	0.89	0.87
DH -76 × 152 × 4.1- U[a]	219	618	618	345	600	LB	0.87	0.76	0.84	0.48
DH -76 × 152 × 4.1- G[a]	224	698	698	640	685	LB	0.94	0.85	0.92	0.86
D − 76 × 102 × 3.2- U	212	445	445	330	N/A	CY	1.21	0.90	N/A	0.90
D − 76 × 102 × 3.2- G	212	496	496	420	N/A	CY	1.24	0.97	N/A	1.05
D − 76 × 102 × 4.8- U	210	459	472	150	N/A	CY	1.12	1.00	N/A	0.37
D − 76 × 102 × 4.8- G	215	529	532	430	N/A	CY	1.25	1.15	N/A	1.01
D − 102 × 102 × 3.2- U	212	416	416	255	N/A	CY	1.21	0.89	N/A	0.74
D − 102 × 102 × 3.2- G	216	477	477	380	N/A	CY	1.26	0.96	N/A	1.00
D − 102 × 102 × 4.8- U	206	473	503	170	N/A	CY	1.19	1.03	N/A	0.43
D − 102 × 102 × 4.8- G	220	537	551	450	N/A	CY	1.14	1.07	N/A	0.96
D − 127 × 127 × 4.8- U	205	457	461	245	N/A	CY	1.16	1.01	N/A	0.62
D − 127 × 127 × 4.8- G	217	523	523	410	N/A	CY	1.22	1.12	N/A	0.96
I-102 × 102 × 6.4- U	196	430	507	140	N/A	CY	1.04	1.05	N/A	0.34
I-102 × 102 × 6.4–450	192	480	546	360	N/A	CY	1.12	1.08	N/A	0.84
I-102 × 102 × 6.4–595	193	440	505	410	N/A	CY	1.15	1.04	N/A	1.07
I-102 × 102 × 6.4- G	192	510	583	370	N/A	CY	1.15	1.15	N/A	0.83
I-102 × 102 × 7.9- U	201	470	560	175	N/A	CY	1.03	1.10	N/A	0.38
I-102 × 102 × 7.9–450	190	525	625	350	N/A	CY	1.12	1.16	N/A	0.75
I-102 × 102 × 7.9–595	191	470	582	425	N/A	CY	1.15	1.15	N/A	1.04
I-102 × 102 × 7.9- G	197	535	644	350	N/A	CY	1.12	1.22	N/A	0.73
I-102 × 102 × 13- U	171	N/A	N/A	150	N/A	N/A	N/A	N/A	N/A	0.31
I-102 × 102 × 13–450	194	N/A	N/A	360	N/A	N/A	N/A	N/A	N/A	0.75
I-102 × 102 × 13–595	195	N/A	N/A	N/A	N/A	N/A	N/A	N/A	N/A	N/A
I-102 × 102 × 13- G	193	N/A	N/A	380	N/A	N/A	N/A	N/A	N/A	0.77

[a] Indicates a repeated test.

5.2. Local buckling behaviour

It is well known that the structural behaviour and load carrying capacity of a stiffened compression element depend on its effective width-to-thickness ratio, supporting condition and residual stress level [8]. For a compression element with a large effective width-to-thickness ratio, local buckling can occur before reaching the yield stress. In this study, the vertical tangent method developed by Roorda and Venkataramaiah [31] and used in Ma et al. [17], was adopted to examine the local buckling behaviour. For six of the 36 stub column specimens, the experimental ultimate loads were lower than the cross-sectional squash loads calculated using the flat and corner coupon yield stresses (i.e. $P_{exp}/P_y^* < 1.00$ in Table 5). Hence, these six stub column specimens experienced local buckling before yielding (LB in Table 5).

To determine the local buckling stresses (σ_{lb}), the strain gauge readings were used to establish the compressive stress-strain relationships of all four faces of an RHS stub column (see Fig. 12 for an example). As shown, the stress-strain curves of the faces subjected to local plate buckling showed a reduction in the compressive strains. For each of the plate elements that failed by local buckling, the stress at the maximum compressive strain was determined as the local buckling stress. Fig. 12 illustrates the determination of the local buckling stress of DH-76 × 102 × 3.2-U. Since the location at which the local buckling initiates may not coincide with where the strain gauges are installed, this method provides an upper bound approximation. The local buckling stresses were normalized by the yield stresses of the corresponding tensile coupons from the flat faces in Table 4. It can be noticed from Fig. 12 that the webs of DH-76 × 102 × 3.2-U (faces 1 and 3) experienced local buckling almost simultaneously. This not only indicates a symmetrical distribution of strength and residual stress properties about the transverse axis, but also substantiates the proper alignment of the stub column within the loading frame. The σ_{lb}-values for the six specimens failed by local buckling are listed in Table 4.

As shown in Table 4, stub column specimen DH-76 × 102 × 3.2-U failed by local buckling during the test. On the other hand, after the application of hot-dip galvanizing, DH-76 × 102 × 3.2-G exhibited compact section behaviour and exceeded its corresponding squash load ($A\sigma_{y,\,f}$). The cross-sectional yield stress of DH-76 × 102 × 3.2-G was 17% higher than that of DH-76 × 102 × 3.2-U. To further substantiate this experimental evidence, two repeated tests was performed (DH-76 × 102 × 3.2-U* vs. DH-76 × 102 × 3.2-G* in Table 4), where after galvanizing the failure mode also changed from local buckling to cross-sectional yielding, and a 16% strength increase was observed. Similar responses were observed when testing: (i) DH-76 × 152 × 4.1-U vs. DH-76 × 152 × 4.1-G, and (ii) DH-76 × 152 × 4.1-U* vs. DH-76 × 152 × 4.1-G*. The hot-dipping process raised on average the local buckling stress by 15%, and an average strength increase of 13% was found. Hence, the application of hot-dip galvanizing, similar to heat treatment, is effective in increasing stub column capacity, delaying local buckling, and can potentially convert a slender cross section to a compact one. The effects of galvanizing on the slender sections under compression will be further discussed by examining the compactness criteria in various design standards in Section 6.

5.3. Proportional limits

One can see the significance of residual stresses over a cross section by superimposing the applied stress on them. As the loading increases, the summation of the applied and residual stresses causes some

Table 5
Comparison of experimental stub column test results with the predicted design values.

Specimen ID	P_{exp} (KN)	Failure mode	P_{exp}/P_y[a]	P_{exp}/P_{CSA}	P_{exp}/P_{EC3}	P_{exp}/P_{AISC}	P_{exp}/P_{DSM}
DH-76 × 76 × 4.8-C-U	1116	CY	1.29	1.36	1.35	1.37	1.37
DH-76 × 76 × 4.8-C-G	1116	CY	1.12	1.17	1.17	1.18	1.18
DH-76 × 102 × 3.2-C-U	666	LB	0.95	1.07	1.09	1.07	1.11
DH-76 × 102 × 3.2-C-G	773	CY	0.96	1.22	1.24	1.21	1.24
DH-76 × 102 × 3.2-C-U[b]	678	LB	1.08	1.09	1.11	1.09	1.13
DH-76 × 102 × 3.2-C-G[b]	784	CY	1.09	1.24	1.26	1.22	1.25
DH-76 × 102 × 4.1-C-U	1052	CY	1.17	1.23	1.24	1.24	1.24
DH-76 × 102 × 4.1-C-G	1109	CY	1.20	1.27	1.27	1.28	1.28
DH-76 × 102 × 4.8-C-U	1276	CY	1.30	1.35	1.36	1.36	1.36
DH-76 × 102 × 4.8-C-G	1241	CY	1.16	1.19	1.20	1.20	1.20
DH-76 × 152 × 4.1-C-U	1043	LB	0.88	1.11	1.12	1.09	1.13
DH-76 × 152 × 4.1-C-G	1169	LB	0.89	1.20	1.22	1.17	1.20
DH-76 × 152 × 4.1-C-U[b]	1052	LB	0.95	1.11	1.13	1.10	1.14
DH-76 × 152 × 4.1-C-G[b]	1189	LB	0.97	1.22	1.24	1.19	1.22
D-76 × 102 × 3.2-C-U	459	CY	1.21	1.27	1.26	1.27	1.27
D-76 × 102 × 3.2-C-G	507	CY	1.24	1.28	1.28	1.29	1.29
D-76 × 102 × 4.8-C-U	679	CY	1.09	1.16	1.15	1.17	1.17
D-76 × 102 × 4.8-C-G	757	CY	1.18	1.25	1.24	1.25	1.25
D-102 × 102 × 3.2-C-U	478	CY	1.18	1.22	1.22	1.23	1.23
D-102 × 102 × 3.2-C-G	539	CY	1.22	1.25	1.24	1.25	1.25
D-102 × 102 × 4.8-C-U	839	CY	1.20	1.26	1.26	1.27	1.27
D-102 × 102 × 4.8-C-G	913	CY	1.13	1.17	1.16	1.17	1.17
D-127 × 127 × 4.8-C-U	969	CY	1.12	1.16	1.16	1.16	1.16
D-127 × 127 × 4.8-C-G	1091	CY	1.17	1.21	1.20	1.21	1.21
Mean $^{DH-CY}$				1.26	1.27	1.27	1.27
COV $^{DH-CY}$				0.058	0.057	0.058	0.058
Mean $^{DH-LB}$				1.16	1.18	1.14	1.18
COV $^{DH-LB}$				0.057	0.055	0.049	0.046
Mean $^{D-CY}$				1.22	1.22	1.23	1.23
COV $^{D-CY}$				0.037	0.036	0.037	0.037

[a] $P_y = A_c \times \sigma_{y,c} + A_f \times \sigma_{y,f}$; $A_f = 2\,[(H - 4\,t)t + (B - 4\,t)t]$, $A_c = A - A_f$.
[b] Indicates a repeated test.

portions of the cross section to yield before others. The resulting behaviour can be analysed using the "effective section" concept [11]. Portions of the cross section that have yielded no longer contribute to the stiffness of the cross section, but still carry their portion of the applied load. Hence, proportional limit is an indicator of the maximum compressive residual stress within a cross section. The proportional limits (σ_p) of all stub columns are listed in Table 4. The proportional limit was determined by fitting a straight line to the elastic portion of the stress-strain curve. The point from which the stress-strain curve starts to deviate from the straight line is identified as the proportional limit (i.e. the stress is no longer proportional to the strain). Representative curves and values are shown in Figs. 13 and 14.

As shown in Table 4, the proportional limits of the direct-formed RHS stub columns are in general much higher than their indirect-formed counterparts. As shown in Figs. 13 and 14, the effects of hot-dip galvanizing and the 450 °C heat treatment per [6,7] on raising the proportional limit are nearly the same. The 595 °C heat treatment per [22] is the most effective among the three in raising the proportional limits. Hence, it may be more suitable for prevention of corner cracking in thick-walled RHS during welding and galvanizing [5].

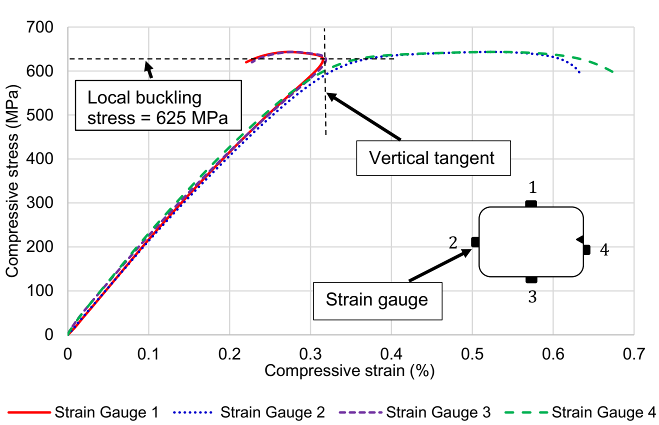

Fig. 12. Vertical tangent method to determine the local buckling stress of DH-76 × 102 × 3.2-U.

6. Evaluation of relevant design provisions

6.1. Design strengths

One objective of this research is to compare the stub column test results of the direct-formed regular- and high-strength RHS with the predicted values using various design standards. For the 24 direct-formed RHS specimens, the unfactored axial compressive resistances based on CSA S16–14 [8], ANSI/AISC 360–10 [14], EN-1993-1-1 [32] and the Direct Strength Method in AISI S100–16 [33] were calculated and shown in Table 5. The mean values and coefficients of variation for high-strength specimens failed in cross-sectional yielding (DH-CY), high-strength specimens failed in local buckling (DH-LB), and regular-strength specimens failed in cross-sectional yielding (D-CY) are also listed in Table 5. As shown, the predictions from various design standards are very conservative for all direct-formed specimens, regardless of the failure modes or the strength grades. In Canada, the steel design standard CSA S16–14 [8] uses two column curves and assigns heat-treated HSS to the upper curve and cold-formed HSS to the lower curve. The former needs to be heat treated to 450 °C or higher for a Class H finish per CSA G40.20/40.21 [7]. Previous research suggested that the column behaviour of a direct-formed RHS is similar to that of an indirect-formed and heat-treated Class H RHS. However, further research is need to develop column design provisions suitable for direct-formed RHS with different strength grades, external dimension-to-thickness ratios, and subjected to different post-cold-forming treatments.

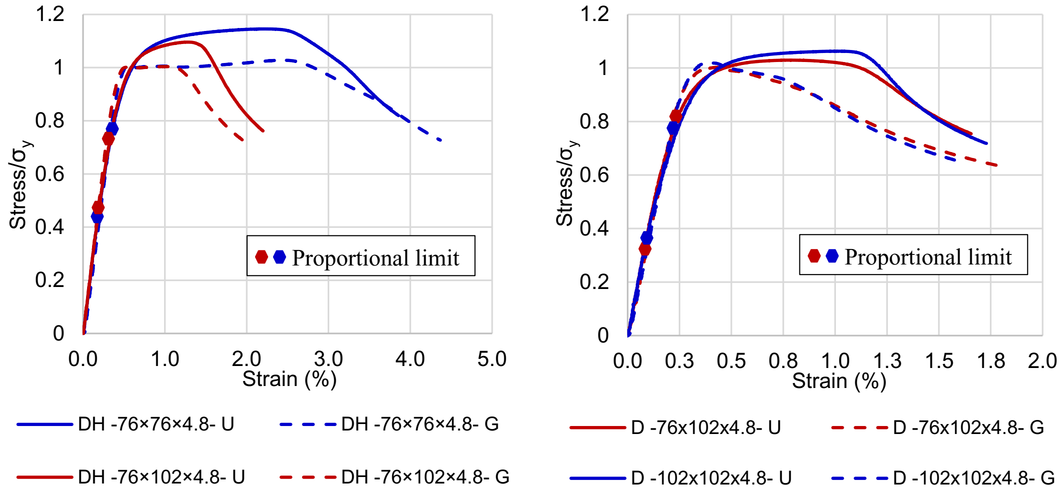

(a) Direct-formed high-strength RHS (b) Direct-formed regular-strength RHS

Fig. 13. Normalized stress-strain responses of direct-formed RHS.

6.2. Yield slenderness limits

Another objective of this research is to examine the compactness criteria in various design standards for the direct-formed RHS. The slenderness limits in various steel design standards are in general established based on the elastic critical local buckling stress of a plate element under consideration. To account for the cross-sectional deterioration due to the existence of compressive residual stress, design standards generally specify limits stricter (i.e. lower) than the theoretical values by imposing a conservative empirical reduction to the latter [11]. Cross-section classification and column design rules in existing steel design standards do not differentiate RHS produced by different cold-forming methods. However, previous research [11–13] showed that the variation in residual stress levels and other mechanical properties in RHS produced by different cold-forming methods can sometimes be significantly different. The direct-forming method, which is the predominant cold-forming method in China and is also used in North America, generally produces lower residual stress. In this section, the experimental results of the direct-formed high-strength RHS (untreated and galvanized) are used to examine the slenderness limits in CSA S16–14 [8] and AISC 360–16 [14] as well as the theoretical elastic critical local buckling stress of a plate element under compression [34].

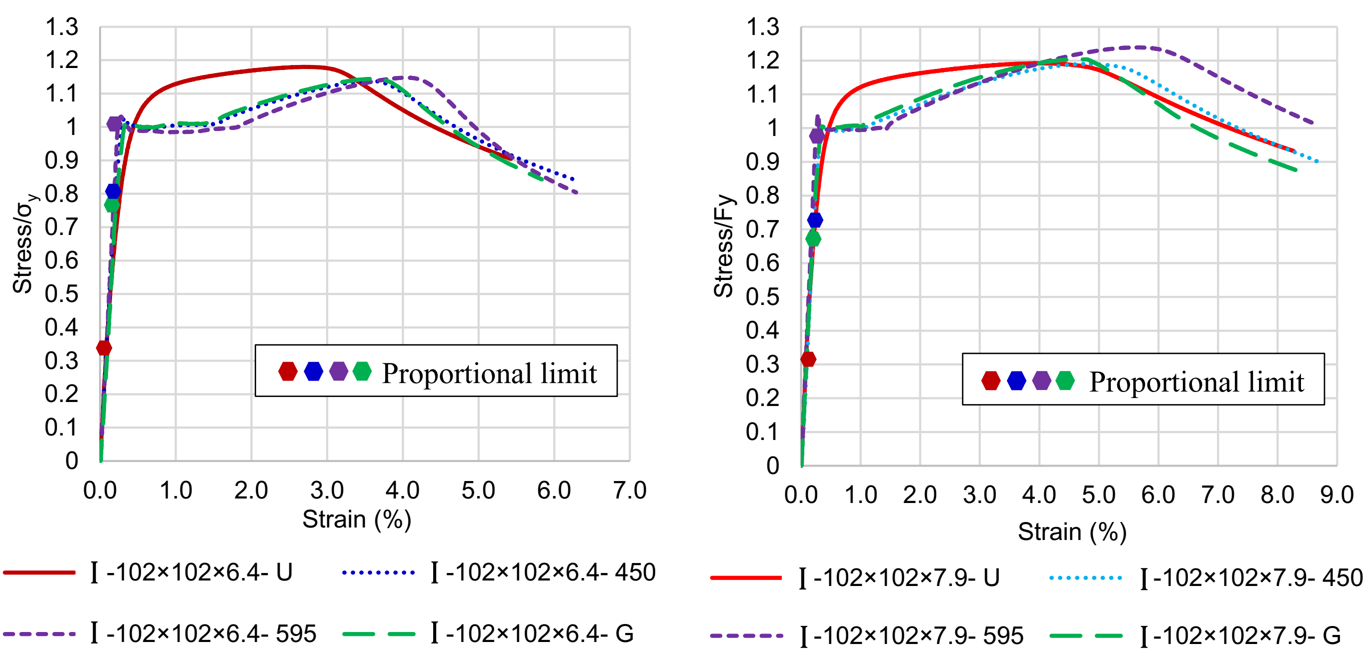

(a) I-102×102×6.4 (b) I-102×102×7.9

Fig. 14. Normalized stress-strain responses of indirect-formed regular-strength RHS.

Table 6
Yield slenderness limits.

Reference	Formula	Normalized yield slenderness limit
CSA S16–14 [8]	$\frac{b}{t} \le \frac{670}{\sqrt{\sigma_y}}$	$\lambda = 1.50$
ANSI/AISC 360–16 [14]	$\frac{b}{t} \le 1.40\sqrt{\frac{E}{\sigma_y}}$	$\lambda = 1.40$
Elastic plate buckling [34,35]	$\frac{b}{t} \le \sqrt{\frac{k\pi^2 E}{12(1-\nu^2)\sigma_y}}$ where $k = 4$ and $\nu = 0.3$	$\lambda = 1.90$

The slenderness limits in various steel design specifications are based on the elastic plate buckling stress [34]. The critical buckling stress (σ_{cr}) of a plate is written as:

$$\sigma_{cr} = \frac{\pi^2 E}{12(1-\nu^2)} \cdot \frac{k}{(b/t)^2} \tag{1}$$

where
E = Young's modulus = 200,000 MPa;
υ = Poisson's ratio = 0.3;
k = local plate buckling coefficient, which accounts for the boundary conditions and loading;
b = width of the stiffened compression element; and.
t = thickness of the plate element.

The b/t limits for RHS under uniform compression in CSA S16–14 [8] and AISC 360–16 [14] are based on [34,35]. It was suggested by [35] that the behaviour of a flat face is similar to a simply supported steel plate under uniform edge compression where k can be taken as 4.0. To standardize the slenderness limits from various references, the width-to-thickness ratios can be normalized into the following format:

$$\lambda = \frac{b}{t\sqrt{\frac{E_f}{\sigma_{y,f}}}} \tag{2}$$

To prevent elastic local buckling from occurring before steel yields, the theoretical normalized slenderness limit, $\lambda = 1.90$ (see Table 6), can be obtained by replacing σ_{cr} in Eq. (1) with σ_y. The formulae for cross section classification for RHS member under compression from CSA S16–14 [8]and AISC 360–16 [14] are shown in Table 6. The two formulae are modified using Eq. (2) to calculate the normalized slenderness limits (λ). It can be seen from Table 6 that, to account for the effects of residual stress and initial geometric imperfection, the λ-values for the design standards [8,14] are lower than the theoretical value of 1.90. It should be noted that the relevant provisions in [8,14] were developed based on testing of indirect-formed RHS. Since the overall levels of residual stresses in the direct-formed (regular- or high-strength) RHS are often considerably lower than their indirect-formed counterparts, the slenderness limit should be closer to 1.90. To assess the performance of the direct-formed high-strength RHS against the yield slenderness limits set out in the design standards, the normalized stub column strengths are plotted against λ in Fig. 15. It can be seen from the figure that:

(1) The application of galvanizing in some cases converted slender sections into compact sections.
(2) According to the linear trend lines, the slenderness limits in CSA S16–14 [8] and AISC 360–16 [14] are excessively conservative for direct-formed high-strength RHS (both untreated and galvanized). Hence, the existing slenderness limits have the tendency to misjudge a nonslender direct-formed section as a slender section, resulting in unnecessary penalty, member strength underestimation and more importantly waste of material.

Hence, further research needs to be conducted to generate more data and to propose realistic slenderness limits for direct-formed RHS (both untreated and galvanized).

7. Conclusions

The main objectives of this research on cold-formed Rectangular Hollow Sections (RHS) were to: (1) quantify the effects of galvanizing, and (2) examine the current industrial practice on heat treatment for a partial residual stress relief for improvement of column behaviour. A total of 112 tensile coupons and 36 stub columns were tested. The specimens were prepared from RHS materials cold-formed by different methods (indirect-forming versus direct-forming), using coil materials with different strength grades. The nominal yield stresses of the materials ranged from 350 to 690 MPa. Twenty one of the 36 RHS specimens were galvanized or heat-treated to different degrees. The stub column test results (e.g. proportional limits, local buckling stresses, yield stresses and ultimate stresses) of the RHS specimens were compared to study the effects of these post-cold-forming processes. It can be concluded based on the available data from this research that:

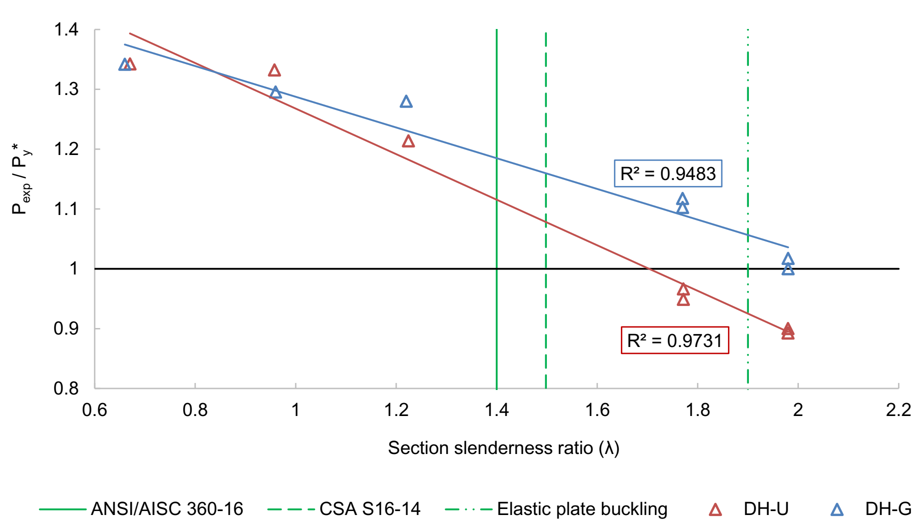

Fig. 15. Comparison of stub column test results for direct-formed high-strength RHS to slenderness limits.

(1) For justification of the use of a higher column curve in CSA S16 [8], a post-cold-forming heat treatment to 450 °C or higher for an ASTM A1085 S1 finish [6], or a CSA G40.20/40.21 Class H finish [7]needs to be performed. According to the experimental evidence in this research, the 30-minute holding time used in the current industrial practice may be excessively long. A 10-minute holding time is suggested based on the findings of this research.
(2) The 595 °C heat treatment per ASTM A143 [22], which consumes more energy than the 450 °C heat treatment per [6,7], has very minor effect on the load carrying capacity of the stub columns, due to the trade-off between residual stress and material strength. Such heat treatment should not be specified for improvement of column behaviour.
(3) Base on the stub column test data in this research, the effects of galvanizing and post-cold-forming heat treatment to 450 °C for 30 min of holding time are similar. Both can be effective in releasing residual stress, delaying local buckling, and can potentially convert a slender cross section to a nonslender section.
(4) Direct-formed RHS (regular strength and high-strength) generally contain a lower overall (cross-sectional) level of residual stress than its indirect-formed counterpart. The column behaviour of a direct-formed RHS can be similar to that of an indirect-formed and heat-treated RHS.

Nomenclature

A	Cross-sectional area of stub column
A_c	Cross-sectional area of corner material
A_f	Cross-sectional area of flat face material
b	Width of stiffened compression element
B	Measured width of RHS
B_n	Nominal width of RHS
E	Young's modulus
E_c	Young's modulus obtained from testing of corner coupon
E_f	Young's modulus obtained from testing of flat coupon
P_{AISC}	Unfactored design strength from ANSI/AISC 360–16
P_{CSA}	Unfactored design strength from CSA S16–14
P_{DSM}	Unfactored design strength from direct strength method
P_{EC3}	Unfactored design strength from EN 1993-1-1
P_{exp}	Experimental ultimate load for stub column
P_y	Theoretical squash load of stub column ($A\sigma_{y,f}$)
H_n	Nominal depth of RHS
H	Measured depth of RHS
k	Plate buckling coefficient
L	Length of stub column
r	Inside corner radius of RHS
R	Outside corner radius of RHS
t	Measured wall thickness
t_n	Nominal wall thickness
α	Slenderness ratio
$\varepsilon_{r,\,c}$	Rupture strain of corner coupon
$\varepsilon_{r,\,f}$	Rupture strain of flat coupon
λ	Normalized slenderness limit
δ_1, δ_2, δ_3	Local geometric imperfection
δ_{max}	Maximum geometric imperfection
σ_{cr}	Elastic critical buckling stress
σ_p	Proportional limit stress
σ_{lb}	Local buckling stress
σ_u	Ultimate stress
$\sigma_{u,c}$	Ultimate stress of corner coupon
$\sigma_{u,f}$	Ultimate stress of flat coupon
σ_y	Yield stress
$\sigma_{y,c}$	Yield stress of corner coupon
$\sigma_{y,f}$	Yield stress of flat coupon

Acronyms

CY	Cross-sectional yielding
HSS	Hollow structural section
LB	Local buckling
RHS	Rectangular hollow section

Author statement

The work has not been published previously.It is not under consideration for publication elsewhere.Thepublication is approved by all authors. If accepted, it will not be published elsewhere in the same form, in English or in any other language, including electronically without the written consent of the copyright-holder.

Declaration of Competing Interest

The authors declare that they have no known competing financial interests or personal relationships that could have appeared to influence the work reported in this paper.

Acknowledgement

Financial support has been provided by the Canadian Institute of Steel Construction (CISC) and the Natural Sciences and Engineering Research Council of Canada (NSERC). Appreciation is extended to Bull Moose Tube and Silver City Galvanizing for their donation of material and service.

References

[1] M. Sun, J.A. Packer, Hot-dip galvanizing of cold-formed steel hollow sections: a state-of-the-art review, Front. Struct. Civ. Eng. 13 (2019) 49–65, https://doi.org/10.1007/s11709-017-0448-0.
[2] AGA, Hot-Dip Galvanizing for Corrosion Protection: A Specifier's Guide, American Galvanizers Association Centennial, CO, USA, 2006.
[3] G. Shi, X. Jiang, W. Zhou, Y. Zhang, Experimental study on overall buckling behavior of Q420 high strength welded galvanized tubes under axial compression, J. Harbin Inst. Technol. 45 (2013) 75–80.
[4] G. Shi, X. Jiang, W. Zhou, T.-M. Chan, Y. Zhang, Experimental investigation and modeling on residual stress of welded steel circular tubes, Int. J. Steel Struct. 13 (2013) 495–508, https://doi.org/10.1007/s13296-013-3009-y.
[5] M. Sun, Z. Ma, Effects of heat-treatment and hot-dip galvanizing on mechanical properties of RHS, J. Constr. Steel Res. 153 (2019) 603–617, https://doi.org/10.1016/J.JCSR.2018.11.012.
[6] ASTM, Standard Specification for Cold-Formed Welded Carbon Steel Hollow Structural Sections (HSS), ASTM A1085/A1085M-15, American Society for Testing and Materials, West Conshohocken, PA, USA, 2015.
[7] CSA, General Requirements for Rolled or Welded Structural Quality Steel/Structural Quality Steel, CSA G40.20-13/G40.21-13, Canadian Standards Association, Toronto, Canada, 2013.
[8] CSA, Limit States Design in Structural Steel, CSA S16-14, Canadian Standard Association, Toronto, ON, Canada, 2014.
[9] S.H. Li, G. Zeng, Y.F. Ma, Y.J. Guo, X.M. Lai, Residual stresses in roll-formed square hollow sections, Thin-Walled Struct. 47 (2009) 505–513, https://doi.org/10.1016/J.TWS.2008.10.015.
[10] L. Tong, G. Hou, Y. Chen, F. Zhou, K. Shen, A. Yang, Experimental investigation on longitudinal residual stresses for cold-formed thick-walled square hollow sections, J. Constr. Steel Res. 73 (2012) 105–116, https://doi.org/10.1016/J.JCSR.2012.02.004.
[11] M. Sun, J.A. Packer, Direct-formed and continuous-formed rectangular hollow sections — comparison of static properties, J. Constr. Steel Res. 92 (2014) 67–78, https://doi.org/10.1016/J.JCSR.2013.09.013.
[12] M. Sun, J.A. Packer, Charpy V-notch impact toughness of cold-formed rectangular hollow sections, J. Constr. Steel Res. 97 (2014) 114–126, https://doi.org/10.1016/J.JCSR.2014.02.005.
[13] M. Sun, J.A. Packer, High strain rate behaviour of cold-formed rectangular hollow sections, Eng. Struct. 62–63 (2014) 181–192, https://doi.org/10.1016/J.ENGSTRUCT.2014.01.023.
[14] ANSI/AISC, Specification for Structural Steel Buildings, ANSI/AISC 360-10, Chicago, IL, USA, 2016.
[15] X.-L. Zhao, A. Heidarpour, L. Gardner, Recent developments in high-strength and stainless steel tubular members and connections, Steel Constr. 7 (2014) 65–72, https://doi.org/10.1002/stco.201410019.

[16] T.-M. Chan, X.-L. Zhao, B. Young, Cross-section classification for cold-formed and built-up high strength carbon and stainless steel tubes under compression, J. Constr. Steel Res. 106 (2015) 289–295, https://doi.org/10.1016/J.JCSR.2014.12.019.
[17] J.L. Ma, T.M. Chan, B. Young, Experimental investigation on stub-column behavior of cold-formed high-strength steel tubular sections, J. Struct. Eng. (United States). 142 (2016), 04015174. https://doi.org/10.1061/(ASCE)ST.1943-541X.0001456.
[18] J. Wang, S. Afshan, N. Schillo, M. Theofanous, M. Feldmann, L. Gardner, Material properties and compressive local buckling response of high strength steel square and rectangular hollow sections, Eng. Struct. 130 (2017) 297–315, https://doi.org/10.1016/J.ENGSTRUCT.2016.10.023.
[19] B. Somodi, B. Kövesdi, Flexural buckling resistance of cold-formed HSS hollow section members, J. Constr. Steel Res. 128 (2017) 179–192, https://doi.org/10.1016/J.JCSR.2016.08.014.
[20] J.-L. Ma, T.-M. Chan, B. Young, Design of cold-formed high-strength steel tubular stub columns, J. Struct. Eng. 144 (2018), 04018063. https://doi.org/10.1061/(ASCE)ST.1943-541X.0002046.
[21] X. Lan, J. Chen, T.-M. Chan, B. Young, The continuous strength method for the design of high strength steel tubular sections in compression, Eng. Struct. 162 (2018) 177–187, https://doi.org/10.1016/J.ENGSTRUCT.2018.02.010.
[22] ASTM, Standard Practice for Safeguarding against Embrittlement of Hot-Dip Galvanized Structural Steel Products and Procedure for Detecting Embrittlement, ASTM A143/A143M-07, American Society for Testing and Materials, West Conshohocken, PA, USA, 2014.
[23] ASTM, Tension Testing of Metallic Materials, ASTM E8/E8M-16a, American Society for Testing and Materials, West Conshohocken, PA, USA, 2016.
[24] Y. Huang, B. Young, The art of coupon tests, J. Constr. Steel Res. 96 (2014) 159–175, https://doi.org/10.1016/J.JCSR.2014.01.010.
[25] J.-L. Ma, T.-M. Chan, B. Young, Material properties and residual stresses of cold-formed high strength steel hollow sections, J. Constr. Steel Res. 109 (2015) 152–165, https://doi.org/10.1016/J.JCSR.2015.02.006.
[26] W.-M. Quach, B. Young, Material properties of cold-formed and hot-finished elliptical hollow sections, Adv. Struct. Eng. 18 (2015) 1101–1114, https://doi.org/10.1260/1369-4332.18.7.1101.
[27] B. Schafer, T. Peköz, Computational modeling of cold-formed steel: characterizing geometric imperfections and residual stresses, J. Constr. Steel Res. 47 (1998) 193–210, https://doi.org/10.1016/S0143-974X(98)00007-8.
[28] B. Young, E. Ellobody, Column design of cold-formed stainless steel slender circular hollow sections, Steel Compos. Struct. 6 (2006) 285, https://doi.org/10.1016/j.jss.2005.11.361.
[29] R.G. Dawson, A.C. Walker, Post-buckling of geometrically imperfect plates, J. Struct. Div. 98 (1972) 75–94.
[30] R.D. Ziemian, Guide to Stability Design Criteria for Metal Structures, John Wiley & Sons, Hoboken, USA, 2010.
[31] J. Roorda, K.R. Venkataramaiah, Analysis of local plate buckling experimental data, 6th Int. Spec. Conf. Cold-Formed Steel Struct., St. Louis, Missouri, 1982.
[32] CEN, Eurocode 3—Design of Steel Structures—Part 1–1: General Rules and Rules for Buildings, BS EN-1993-1-1, British Standards Institution, London, UK, 2005.
[33] AISI, North American Specification for the Design of Cold-Formed Steel Structural Members, AISI S100–16, American Iron and Steel Institute, Washington, DC, 2016.
[34] S.P. Timoshenko, J.M. Gere, Theory of Elastic Stability, 2. ed. McGraw-Hill, Auckland, 1963.
[35] E.E. Lundquist, Local instability of symmetrical rectangular tubes under axial compression, National Advisory Committee for Aeronautics, report no. 686, 1939.